A Method-of-Moments Study of Strip Dipole Antennas in Rectangular Waveguide

Andrew R. Adams, Roger D. Pollard, *Fellow, IEEE,* and Christopher M. Snowden, *Fellow, IEEE*

***Abstract*—A theoretical and experimental study of strip dipole antennas located on a supporting dielectric slab mounted transversely in rectangular waveguide is presented. Galerkin's method is used in the full-wave solution of an integral equation for each antenna's surface-current density using the Green's function for the slab-loaded waveguide. The paper is motivated by the need for multiport-network models to aid the development of multiple-device power-combining circuits in rectangular waveguide. The design data presented here for single antennas should prove useful for planar-mixer and oscillator circuits. The presence of slab modes is noted and the slab-mode resonant frequencies are predicted. Validation of the numerical models is provided by scattering experiments on the shorted antennas, and excellent agreement is obtained in the range of 8.0–12.5 GHz.**

***Index Terms*— Antennas, method of moments (MoM), quasi-optics, waveguide.**

I. Introduction

PLANAR antennas for the coupling of RF energy to and from an active device in an enclosed environment are of significant interest as an alternative to circular posts and for low-loss power-combining, particularly at millimeter-wave frequencies. Planar circuits have the well-known advantages of reduced manufacturing cost, repeatable impedance behavior from precise fabrication methods, and the potential for monolithic integration with active devices.

Arrays of planar antennas have been used in quasi-optical oscillator power combiners [1]–[3] and amplifiers [4]–[6] which can provide highly efficient power combining by eliminating hybrid splitting and combining networks. A variation is radiative power combining in rectangular waveguide, which has been used in recent designs [7], [8] and is of interest since the enclosure provides robustness as well as a conducting boundary for the removal of heat. Fig. 1 shows a multiple-oscillator power combiner with a section of rectangular waveguide holding a transverse dielectric slab supporting an array of strip dipole antennas. The full-wave analysis without unit-cell or infinite-array assumptions of the strip dipole array leading to a multiport-network model is presented in this paper together with design data for the driving-point impedance of single-antenna circuits.

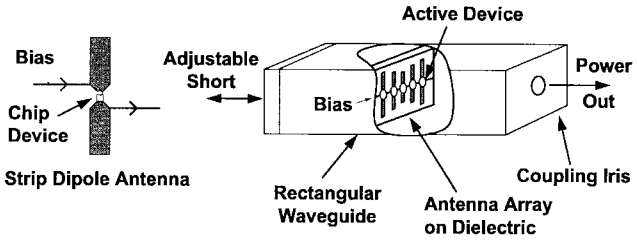

Fig. 1. Strip dipole-antenna array in rectangular waveguide with hybrid oscillators configured for power combing.

Single strips in rectangular waveguide and planar quasi-optical arrays have been successfully modeled in the past. Eisenhart and Khan [9] applied the induced-EMF method to determine the driving-point impedance of a flat strip in infinite rectangular waveguide from an assumed current-density distribution on its surface, extending the analysis to circular posts with an empirically determined correction factor. Quasi-optical arrays have been successfully characterized to 60 GHz using this method with a unit-cell approach based on an infinite-array assumption and TEM-mode excitation [2], [6].

There has been much work on the full-wave analysis of boxed circuits incorporating planar transmission lines on one or more dielectric layers [10]–[13] using the method of moments (MoM) in either the spatial or spectral domains. Li [13] presented the Green's function for semi-infinite rectangular waveguide filled with a multilayered media, and Hashemi–Yeganeh [14] analyzed the electrical behavior of thin metallic posts in rectangular waveguide using the MoM. However, in all these previous analyses, the problems are formulated with fixed waveguide terminations or ignore the effect of the supporting dielectric.

In this paper, we first detail the integral-equation formulation and the derivation of the necessary Green's function for the rectangular waveguide loaded with transverse dielectric slab. The MoM solution of the integral equation leading to a network model for the antenna array is then presented, followed by an examination of the electromagnetic behavior of single-strip dipole antennas showing their behavior as a function of frequency, dielectric, and geometric parameters. The conditions under which dielectric slab modes are strongly excited are also discussed. The computational approach and the results from scattering experiments are presented as validation of the theoretical analysis.

Manuscript received May 14, 1997; revised June 20, 1997. The work of A. R. Adams was supported in part by the Hewlett-Packard Santa Rosa Systems Division, in part by the U.K. Government ORS Awards scheme, and in part by the IEEE Microwave Theory and Techniques Society under a Graduate Fellowship.

A. R. Adams was with the Microwave and Terahertz Technology Research Group, Department of Electronic and Electrical Engineering, University of Leeds, Leeds LS2 9JT, U.K. He is now with Standard Communications Pty Ltd., Gladesville N.S.W., 2111 Australia.

R. D. Pollard and C. M. Snowden are with the Institute of Microwaves and Photonics, School of Electronic and Electrical Engineering, University of Leeds, Leeds LS2 9JT, U.K.

Publisher Item Identifier S 0018-9480(97)07111-1.

II. MoM Analysis

The total field at any point in the waveguide is the superposition of the total elemental current-source field and is frequently written as

$$\mathbf{E}(\mathbf{r}) = -j\omega\mu_0 \int_V \overline{\mathbf{G}}(\mathbf{r}|\mathbf{r}') \cdot \mathbf{J}(\mathbf{r}')\, dV' \tag{1}$$

where $\overline{\mathbf{G}}(\mathbf{r}|\mathbf{r}')$ is the Green's function and $e^{j\omega t}$ time dependence is assumed. Boldface denotes a vector quantity and the over-bar denotes a dyadic. When some of the components of $\mathbf{E}(\mathbf{r})$ are known such as on perfectly conducting surfaces, the only unknown in (1) is the surface-current density $\mathbf{J}(\mathbf{r}')$. However, a general analytical solution of this equation is impossible. In specific cases where the geometry of the problem permits $\overline{\mathbf{G}}(\mathbf{r}|\mathbf{r}')$ to be calculated, the problem is reduced to the evaluation of $\mathbf{J}(\mathbf{r}')$, from which $\mathbf{E}(\mathbf{r})$ is determined by substitution into (1) and $\mathbf{H}(\mathbf{r})$ from $\mathbf{E}(\mathbf{r})$ by recourse to Maxwell's equations.

Many techniques are available to discretize the continuous integral equation and achieve a numerical solution for $\mathbf{J}(\mathbf{r}')$, with the most popular being the MoM [15]. Problems such as this, in which the Green's function can be derived, can be solved more rapidly using the MoM than a volume FEM, the finite-difference time domain (FDTD) method, or the transmission-line matrix method, all of which require meshing of the total volume of the structure.

The MoM analysis which follows is restricted to rectangular strips, although extension to arbitrary shapes is possible with the aid of a suitable meshing algorithm. It is assumed throughout that all metal surfaces are perfect conductors, in which case the electric-field tangential to these surfaces $\mathbf{E_t}(\mathbf{r}) = \mathbf{0}$. Then, the only areas over which nonzero $\mathbf{E_t}(\mathbf{r})$ exists are the feed regions of the antennas. This then gives the well-known electric-field integral equation (EFIE) for the surface of each antenna:

$$-j\omega\mu_0 \int_V \overline{\mathbf{G}}(\mathbf{r}|\mathbf{r}') \cdot \mathbf{J}(\mathbf{r}')\, dV' = \begin{cases} -\mathbf{E_f}(\mathbf{r}), & \text{at the feeds} \\ 0, & \text{elsewhere.} \end{cases} \tag{2}$$

The components of $\overline{\mathbf{G}}(\mathbf{r}|\mathbf{r}')$ involving z are not required, as it has been assumed that the antennas have no $\hat{z}$-extent. Throughout the following discussion, the excitation is assumed to be $\hat{x}$-directed. If the excitation and geometric conditions are such that the surface-current density is well-approximated by the current in the $\hat{y}$-direction alone, then only the $\mathbf{G_{yy}}(\mathbf{r}|\mathbf{r}')$ component of the dyadic Green's function is retained in (2). The reaction inner product

$$\langle \mathbf{E_f}(\mathbf{r}), \mathbf{J}(\mathbf{r}) \rangle \cong \int_S \mathbf{E}(\mathbf{r}) \cdot \mathbf{J}(\mathbf{r})\, dS \tag{3}$$

where $\mathbf{E}(\mathbf{r})$ is the electric field and $\mathbf{J}(\mathbf{r})$ the current density is a suitable inner product for the MoM [16] and is used in the following analysis.

A. Decomposition into Linear Equations

The unknown surface-current density on each antenna is expanded in piecewise sinusoidal functions S and pulse functions P as follows:

$$J_x(x, y) = \sum_{i=1}^{P-1} J_{xx_i} S(x) \sum_{j=1}^{Q} J_{yx_j} P(y) \tag{4}$$

$$J_y(x, y) = \sum_{i=1}^{P} J_{xy_i} P(x) \sum_{j=1}^{Q-1} J_{yy_j} S(y) \tag{5}$$

where

$$S(y) = \begin{cases} \dfrac{\sin\{k_0[y' - y_0 - (A-1)\Delta y]\}}{\sin(k_0 \Delta y)} \\ \qquad y_0 + (A-1)\Delta y \le y' \le A\Delta y \\ \dfrac{\sin\{k_0[(A+1)\Delta y - y' + y_0]\}}{\sin(k_0 \Delta y)} \\ \qquad y_0 + A\Delta y \le y' \le (A+1)\Delta y \end{cases} \tag{6}$$

and

$$P(y) = \begin{cases} 1 & (A-1)\Delta y \le y' \le A\Delta y \\ 0 & \text{otherwise.} \end{cases} \tag{7}$$

In both (6) and (7), A is an integer ranging over the P–$\hat{x}$ sections and Q–$\hat{y}$ sections on the antenna, $k_0 = 2\pi/\lambda_0$ and $(x_0, y_0) = (\alpha - w, \beta - l)$ is the strip origin where 2l is the total antenna length, $2w$ the total width, and (α, β) the center of the strip. These expressions are now substituted into the coupled EFIE, and the integrals carried out over the surface of each antenna in the array. The electric-field expressions so generated are then *tested* through the reaction integral in (3), by applying Galerkin's method. This yields a matrix equation of the form

$$\begin{bmatrix} \begin{pmatrix} Z^1_{1_{xx}} & Z^1_{1_{xy}} \\ Z^1_{1_{yx}} & Z^1_{1_{yy}} \end{pmatrix} & \cdots & \begin{pmatrix} Z^1_{w_{xx}} & Z^1_{w_{xy}} \\ Z^1_{w_{yx}} & Z^1_{w_{yy}} \end{pmatrix} \\ \vdots & \ddots & \vdots \\ \begin{pmatrix} Z^w_{1_{xx}} & Z^w_{1_{xy}} \\ Z^w_{1_{yx}} & Z^w_{1_{yy}} \end{pmatrix} & \cdots & \begin{pmatrix} Z^w_{w_{xx}} & Z^w_{w_{xy}} \\ Z^w_{w_{yx}} & Z^w_{w_{yy}} \end{pmatrix} \end{bmatrix} \begin{bmatrix} J_{1_x} \\ J_{1_y} \\ \vdots \\ J_{w_x} \\ J_{w_y} \end{bmatrix} = \begin{bmatrix} \langle E_1, J_1 \rangle \\ \langle E_2, J_2 \rangle \\ \vdots \\ \langle E_{w-1}, J_{w-1} \rangle \\ \langle E_w, J_w \rangle \end{bmatrix} \tag{8}$$

where the submatrices are defined explicitly in Appendix B. In general, $Z^j_{i_{xy}}$ are the elements due to the x-component of the $\hat{y}$-directed electric field from the current on antenna i having been tested with the current elements on antenna j. The square matrix in (8) is known as the *reaction matrix*. The solution vector $[J]$ is obtained by solving the matrix equation from which the electromagnetic behavior of the array can be fully determined.

B. The Feed Model

For the center-fed dipole antennas used in this paper, it was felt that the capacitance of the gap was likely to have significant influence on the electrical performance of the antennas and thus should be incorporated in the electromagnetic analysis. This was achieved by using a finite-gap excitation model rather than a delta-gap model, forcing the excitation to have a constant value over the gap.

The localized nature of the basis functions means that the only nonzero elements of the excitation matrix are those which overlap with the excitation region. For the case of multiple excitations, as in an array, the correct phase at each port must be maintained through $\mathbf{E_f}(\mathbf{r}')$.

For uniform excitation we have the general form for the reaction with a piecewise sine and pulse basis element as follows:

$$\langle \mathbf{E_f}(\mathbf{r}), \mathbf{J}(\mathbf{r})\rangle = \int_{y_0+(A-1)\Delta y-g}^{y_0+(A+1)\Delta y+g} \int_{x_0+(B-1)\Delta x}^{x_0+B\Delta x} \times S(y, \Delta y, A)P(x, \Delta x, B)\, dy\, dx \quad (9)$$

where it is assumed that the excitation is $\hat{y}$-directed and A and B are integers referring to each basis function overlapping with the feed region.

C. The Green's Function $\overline{\mathbf{G}}(\mathbf{r}|\mathbf{r}')$

The electric-field Green's function is the field arising from an arbitrarily located delta-function current source in the rectangular waveguide loaded with a transverse dielectric slab. The presence of the dielectric slab leads to multiple reflections necessitating modification to the empty infinite rectangular-waveguide Green's function of Appendix A. The reflections from the dielectric slab are mode-dependent, although there is no higher order mode generation at the dielectric interfaces. Hence, the same mode set which fully describes the fields in the empty guide also does so inside the dielectric. The new Green's function $\overline{\mathbf{G}}(\mathbf{r}|\mathbf{r}')$ can be written as

$$\overline{\mathbf{G}}(\mathbf{r}|\mathbf{r}') = \xi_{\rm te}\overline{\mathbf{G}}^{\rm te}(\mathbf{r}|\mathbf{r}') + \xi_{\rm tm}\overline{\mathbf{G}}^{\rm tm}(\mathbf{r}|\mathbf{r}') \quad (10)$$

where $\overline{\mathbf{G}}_{\mathbf{i}}(\mathbf{r}|\mathbf{r}')$ is the infinite-waveguide Green's function composed of its TE and TM components

$$\overline{\mathbf{G}}_{\mathbf{i}}(\mathbf{r}|\mathbf{r}') = \overline{\mathbf{G}}^{\rm te}(\mathbf{r}|\mathbf{r}') + \overline{\mathbf{G}}^{\rm tm}(\mathbf{r}|\mathbf{r}'). \quad (11)$$

The parameters $\xi_{\rm te}$ and $\xi_{\rm tm}$ are found by field matching at the dielectric interfaces. If ϵ is the relative permittivity of the dielectric, and γ_1 is the complex component of the propagation constant in the air-filled guide and γ_2 is that in the dielectric filled guide of the same cross section, then the air-dielectric reflection coefficients are

$$\rho_{\rm te1} = \frac{\gamma_1-\gamma_2}{\gamma_1+\gamma_2}\,\rho_{\rm t1} = \frac{\gamma_2-\epsilon\gamma_1}{\gamma_2+\epsilon\gamma_1} \quad (12)$$

and the associated transmission coefficients

$$t_{\rm te1} = \frac{2\gamma_1}{\gamma_1+\gamma_2}\,t_{\rm t1} = \frac{2\gamma_2}{\gamma_2+\epsilon\gamma_1}. \quad (13)$$

Similarly, the dielectric–air reflection coefficients

$$\rho_{\rm te2} = \frac{\gamma_2-\gamma_1}{\gamma_1+\gamma_2}\,\rho_{\rm t2} = \frac{\epsilon\gamma_1-\gamma_2}{\epsilon\gamma_1+\gamma_2} \quad (14)$$

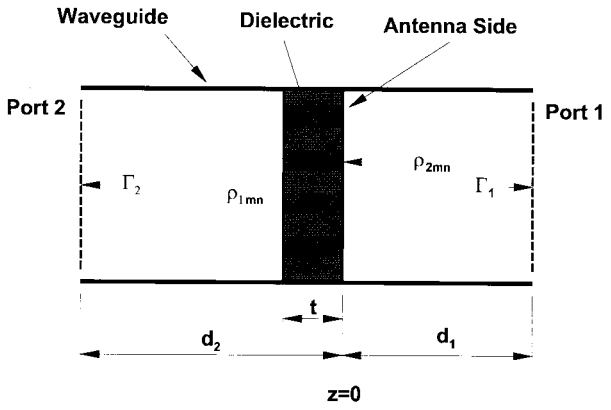

Fig. 2. Geometry for the derivation of the modified Green's function.

and the associated transmission coefficients

$$t_{\rm te2} = \frac{2\gamma_2}{\gamma_1+\gamma_2}\,t_{\rm t2} = \frac{2\epsilon\gamma_1}{\epsilon\gamma_1+\gamma_2}. \quad (15)$$

In this calculation, the Green's function in the plane of the antenna array ($z = 0$) is of interest. Further, the effect of the waveguide terminations must be incorporated into the modified Green's function. Eisenhart and Kahn [9] produced such an expression by considering the standing wave at any point in the guide, though they were only considering the effect on propagating modes. However, the expression is perfectly valid for nonpropagating (evanescent) modes, and is shown in (16) at the bottom of the page, where the dimensions d_1 and d_2 are shown in Fig. 2. In (16), $\rho_{1\rm mn}$ is the mode-dependent reflection coefficient from the plane of the antennas toward port 1 and $\rho_{2\rm mn}$ is that toward port 2. These reflection coefficients are found by considering the multiple-wave reflections at the air–dielectric and dielectric–air interfaces using (12)–(15). It is assumed that the terminations on ports 1 and 2 do not interact with the nonpropagating modes, although such influence can be accommodated without modification to the general theory. Therefore, $\rho_{1\rm mn}$ need only be calculated for the propagating modes in the waveguide. However, the presence of the dielectric requires that the calculations for $\rho_{2\rm mn}$ be made for each mode and is calculated for TE modes by

$$\rho_{2\rm mn} = (S_{11})_{mn} + \frac{(S_{21})^2_{mn}\Gamma_l}{1-(S_{11})_{mn}\Gamma_l} \quad (17)$$

where each scattering term is found by summing an infinite geometric series as follows:

$$\begin{aligned}(S_{11})_{mn} &= \rho_{\rm te1} + \rho_{\rm te2}t_{\rm te1}t_{\rm te2} \\ &\quad \times e^{-2\gamma_{mn2}t}\left\{1+\frac{\rho^2_{\rm te2}e^{-2\gamma_{mn2}t}}{1-\rho^2_{\rm te2}e^{-2\gamma_{mn2}t}}\right\} \\ (S_{21})_{mn} &= t_{\rm te1}t_{\rm te2} \\ &\quad \times e^{-\gamma_{mn2}t}\left\{1+\frac{\rho^2_{\rm te2}e^{-2\gamma_{mn2}t}}{1-\rho^2_{\rm te2}e^{-2\gamma_{mn2}t}}\right\} \\ \Gamma_l &= \Gamma_2 e^{-2\gamma_{mn1}d_2}\end{aligned} \quad (18)$$

$$\left.\begin{matrix}\xi_{\rm te}\\ \xi_{\rm tm}\end{matrix}\right\} = \frac{1+\rho_{1\rm mn}e^{-2\gamma_{mn}d_1}+\rho_{2\rm mn}e^{-2\gamma_{mn}d_2}+\rho_{1\rm mn}\rho_{2\rm mn}e^{-2\gamma_{mn}(d_1+d_2)}}{1-\rho_{1\rm mn}\rho_{2\rm mn}e^{-2\gamma_{mn}(d_1+d_2)}} \quad (16)$$

where the equivalent expressions for TM modes take the same form. With these expressions and (16), the necessary modifications of the infinite-waveguide Green's function can be made and the MoM calculation carried out for a given substrate and waveguide terminations.

D. Array Network Parameters

The full set of network parameters can be obtained from a single reaction matrix by calculating the current-density solution under different excitation conditions. For a single antenna, the current over the region of excitation is defined as

$$I_0 = \int_{-w}^{w} J_y(x)\,dx \tag{19}$$

where the excitation is assumed to be $\hat{y}$ directed. The current-density solution is a piecewise approximation to the true continuous current and is

$$\hat{I}_0 = \sum_{i=1}^{P} J_{xy_i}(x, y=\alpha)\Delta x \tag{20}$$

which, for unit voltage excitation gives by definition

$$Z_{\text{in}} = \frac{1}{\hat{I}_0}. \tag{21}$$

To calculate the full $W \times W$ network matrix for an array of W antennas, W current-density solutions are required. If the vector $\tilde{i}^k$ of currents at each antenna port is the solution for unit excitation at antenna k and all other antennas shorted (zero $\mathbf{E}(\mathbf{r})$ over the feed region), then augmenting the W solutions yields the matrix equation

$$[Z][\tilde{i}^1 \cdots \tilde{i}^W] = [I] \tag{22}$$

where $[I]$ is the identity matrix. If an admittance form $[Y]$ is required then $[Y] = [Z]^{-1} = [\tilde{i}^1 \cdots \tilde{i}^W]$.

III. Computational Detail and Convergence Behavior

For convergence of the numerical calculations both the number of subsections used in the approximation of the antenna's surface-current density and the number of waveguide modes used in the reaction calculation must each be closely monitored. These factors are related so that if a larger number of subsections are used on each antenna for a closer approximation to the true surface-current density then the number of waveguide modes used in each reaction calculation must be modified accordingly. In general, the smaller the subsection area, the greater the number of modes required in the evaluation of the reaction integral. This increases the already greater computational load due to the increased number of subsections on each antenna.

Each element of the reaction matrix requires the evaluation of the doubly-infinite series involving both TE- and TM-mode contributions, as shown in Appendix B. These series converge in a nonuniform way, and so truncation for a specific error bound is impossible. Instead, one must monitor the series in progressive intervals and decide whether the change to the summand is small enough for the summation to be halted. The strategy adopted here is to check over a predefined interval, check the convergence length, check that the relative change in the series elements is less than some number, and check the relative precision. If the change is smaller than the adopted relative precision for at least a number of elements equal to the convergence length, then the summation is halted and evaluation of the next reaction-matrix element proceeds. We find that setting the convergence length to 10 gives stable numerical results with the precision adjusted according to the number of subsections used on each antenna.

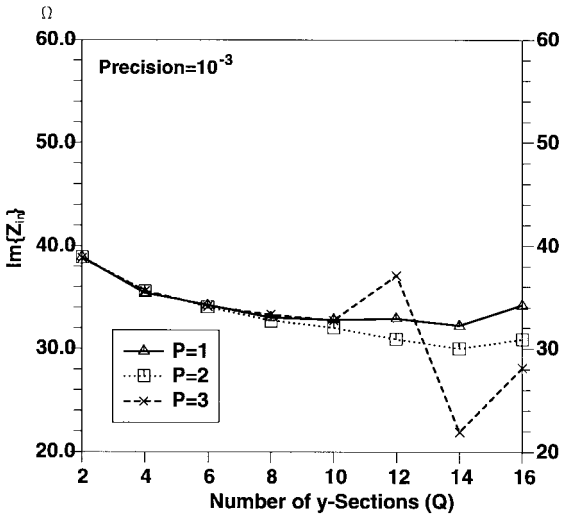

Fig. 3. The variation of antenna input impedance with P and Q and precision $= 10^{-3}$.

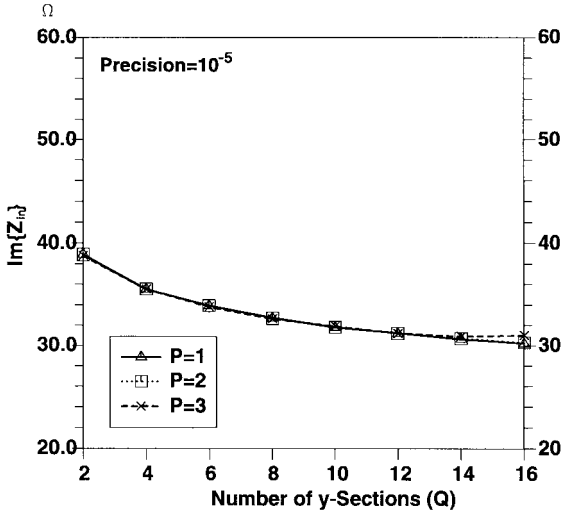

Fig. 4. The variation of antenna input impedance with P and Q and Precision $= 10^{-5}$.

Figs. 3 and 4 show how the real component of antenna input impedance varies with the number of antenna subsections. In these two figures, variation from 2 to 16 $\hat{y}$-sections (Q) with 1–3 $\hat{x}$ sections (P) is shown. It can be seen that associated with a given subsectional area $\Delta x\,\Delta y$ is a minimum precision for good convergence. For example, in Fig. 3 it can be observed that for $P = 1$ or 2 and a precision of 10^{-3}, the real part of input impedance approaches a steady value as Q increases.

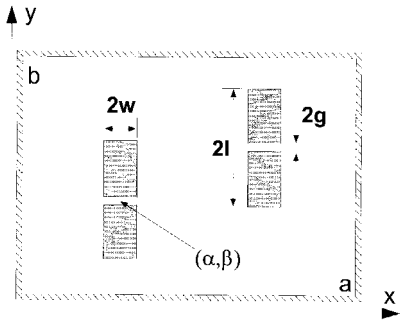

Fig. 5. Antenna and waveguide geometry for the MoM calculations.

However, when $P = 3$ the results of the MoM calculation become erratic with increasing Q. This is because as the subsectional area is reduced with larger values of P and Q, the reaction-matrix series become more slowly converging and at a precision of 10^{-3} the series have not adequately converged when the summation is halted. When a precision of 10^{-5} is used, good convergence behavior is observed, as shown in Fig. 4. Dunleavy and Katehi [17] also observed this behavior in their analysis of boxed microstrip circuits. They called this effect "the erratic current condition," yet the effect, rather than being erratic, appears due to their choice of a modal truncation point being too small for their smallest subsection sizes.

IV. Impedance Calculations

In the following simulations we consider the behavior at 10 GHz of a representative antenna 8-mm long and 1-mm wide fabricated on 0.010-in-thick $\epsilon_r = 2.2$ material and mounted in WR-90 rectangular waveguide with both waveguide ports terminated in Z_{TE} (no reflections)—a configuration subsequently referred to as the *standard antenna*. Where simulations are performed with different geometries, reference is made to the changes. The general geometry is shown in Fig. 5.

The impedance behavior of these waveguide-housed antennas is a function both of the antenna and substrate properties as well as the waveguide terminations. Although the height of standard rectangular waveguide is less than $\lambda_0/4$, resonant behavior is observed if the antenna length and effective relative permittivity of the substrate give an effective antenna length of $\lambda_0/2$ at a particular frequency. Although such a resonant antenna may be useful in some instances, we are more concerned with broad-band applications, and so the results which follow concentrate on the nonresonant properties of these antennas. In addition, the results presented here are for standard WR-90 rectangular waveguide. Of course, other frequency bands and waveguide sizes are of interest, but the general results hold with appropriate scaling.

Fig. 6 shows the frequency response of a standard antenna from 8.0 to 12.5 GHz for different substrate permittivities. The input reactance of the antenna is strongly capacitive at the lower end of the frequency range, indicating coupling primarily to TM_{mn} rather than TE_{mn} evanescent modes. A strong dependence of input reactance on the permittivity is observed in these simulations, the reactance becoming more inductive as the substrate permittivity is increased. Much of

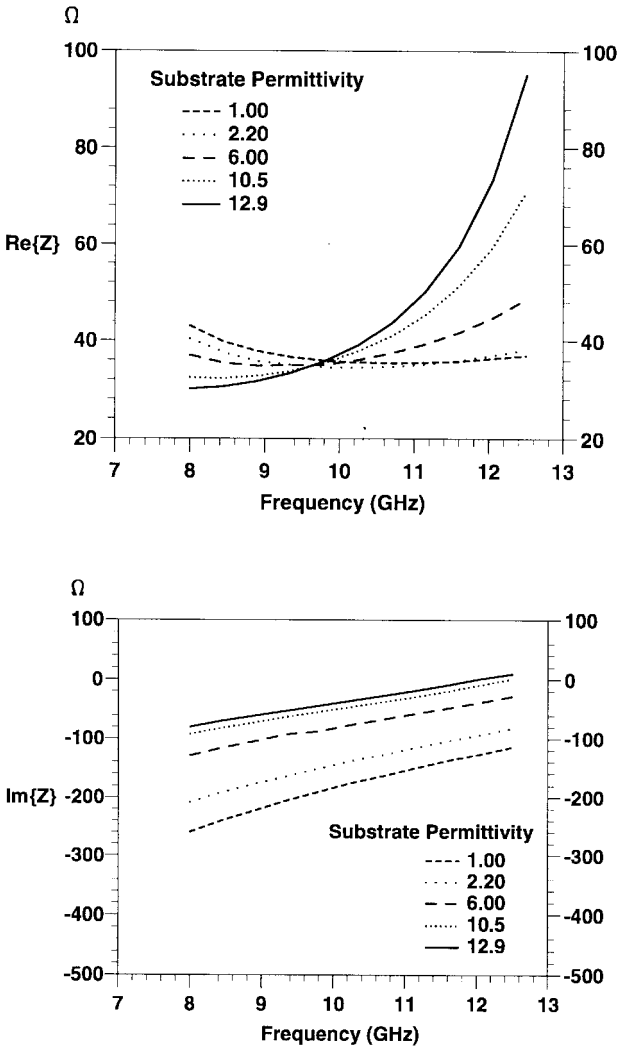

Fig. 6. The real and complex part of input impedance of a strip dipole antenna from 8.0 to 12.5 GHz for different substrate permittivities.

the same behavior is seen in Fig. 7 as the substrate thickness is increased, with a commensurate rise in the effective relative permittivity. For a particular combination of permittivity, thickness, and length, the antenna becomes resonant.

The antenna length appears to have the strongest effect on the input impedance, as shown in Fig. 8. Very short antennas are strongly capacitive in agreement with the results of Eleftheriades *et al.*, who analyzed the behavior of a strip dipole used to excite a rectangular horn antenna. The width of the strip also has a significant effect on the input impedance of these strip antennas, as shown in Fig. 9.

The transverse position of the antenna also strongly influences its input impedance. The input resistance is directly related to the coupling to the propagating modes in the waveguide—in this case, solely the TE_{10} mode. In the absence of a dielectric, the variation of resistance with transverse position follows the expected $\sin(\pi x/a)$ form and is shown in Fig. 10. However, on higher permittivity substrates the trend becomes more complex as the antenna can excite more than one propagating mode in the dielectric. The input reactance also displays a strong dependence on transverse position—especially on

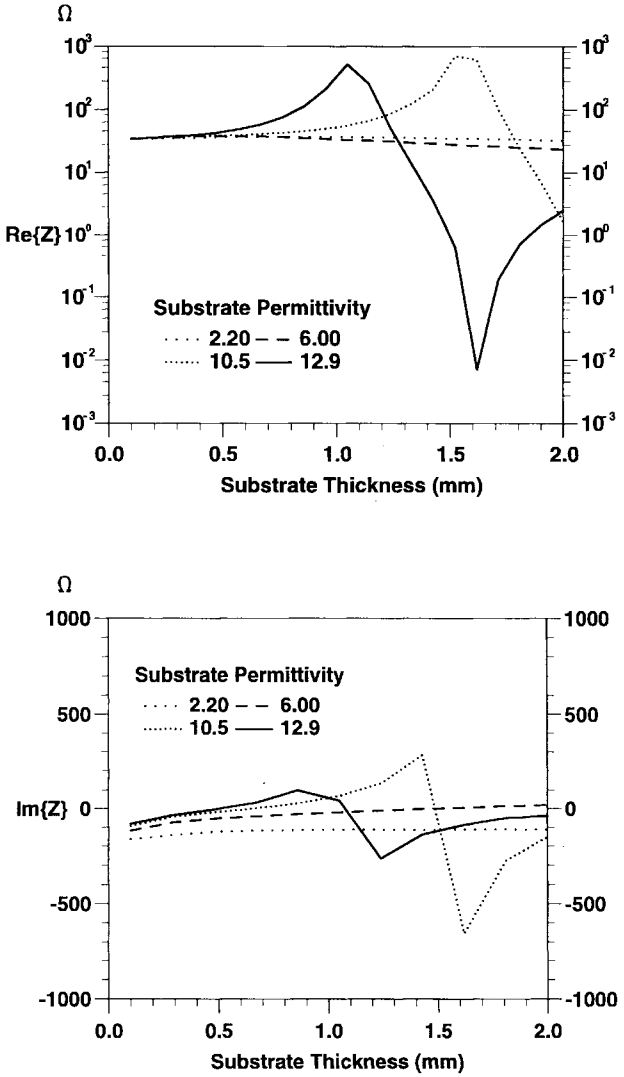

Fig. 7. The real and complex part of input impedance of a strip dipole antenna for different strip thicknesses and permittivities.

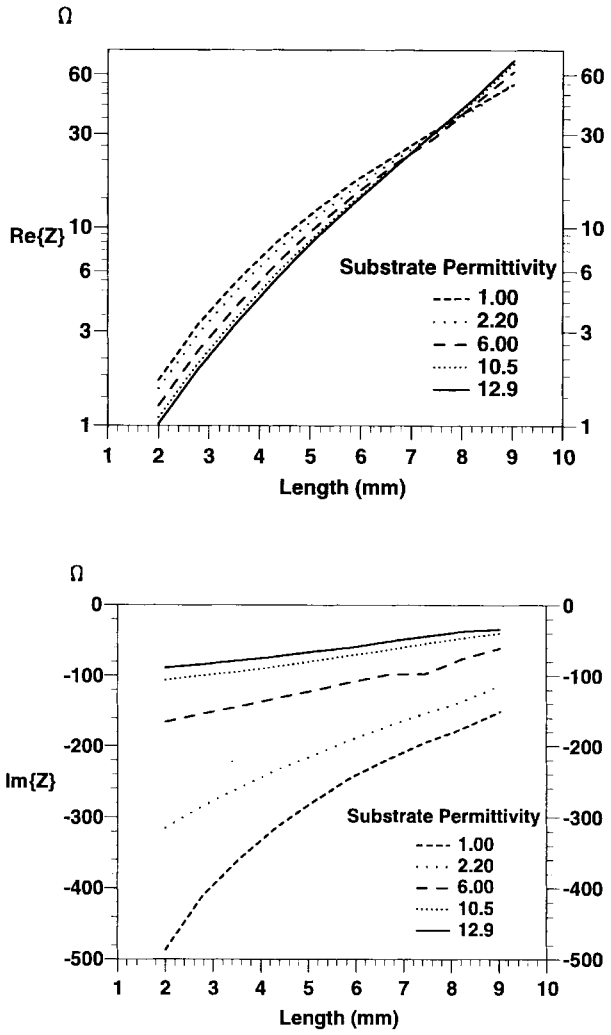

Fig. 8. The real and complex part of input impedance of a strip dipole antenna for different strip lengths and substrate permittivities. Note that the real part of the input impedance is shown on a log scale.

high permittivity substrates—and is also strongly influenced by the proximity of the antenna to the waveguide walls.

V. Dielectric-Slab Modes

The presented numerical analysis is based entirely on the rectangular waveguide modes and assumes propagation as $e^{-\gamma z}$. However, under certain conditions, a current source on the surface of the dielectric will excite one or more transverse slab modes. These are generally undesirable as they represent energy loss as well as causing unwanted coupling between electrically distant antennas. Although the excitation of slab modes is excluded from the general analysis presented in this paper, it is possible to determine those frequencies where the coupling to a slab mode becomes strong such as when the transmission line formed by the transverse dielectric shorted at each end becomes resonant.

The magnetic field $\mathbf{H}(\mathbf{r})$ forms a loop around the antennas in such a way as to suggest coupling predominantly to TE- rather than TM-slab modes. The lowest order mode TE_0 propagates at all frequencies and has a propagation constant k_{xs} given by

$$k_{xs}^2 = k_d^2 - u^2 \tag{23}$$

where u is the solution of the equation

$$\frac{ut}{2} \tan \frac{ut}{2} = \frac{t}{2} \sqrt{k_d^2 - k_0^2 - u^2} \tag{24}$$

and where t is the dielectric thickness and $k_d = k_0\sqrt{\epsilon_r}$ [19]. Solving for k_{xs} and searching for the frequency where $k_{xs}a = 2\pi$, where $a = 22.86$ mm for WR-90 waveguide produces the set of curves shown in Fig. 11. For example, a 1-mm-thick $\epsilon_r = 10.5$ substrate will show a transverse resonance at approximately 9.8 GHz.

VI. Experimental Validation

Accurate measurement of the driving-point impedance of these strip dipole antennas is a difficult task. One approach is to feed a narrow coaxial transmission line through a waveguide wall to the feed point for a direct measurement [9]. However, for a planar structure, such a method presents significant calibration difficulties as well as introducing uncertainties into

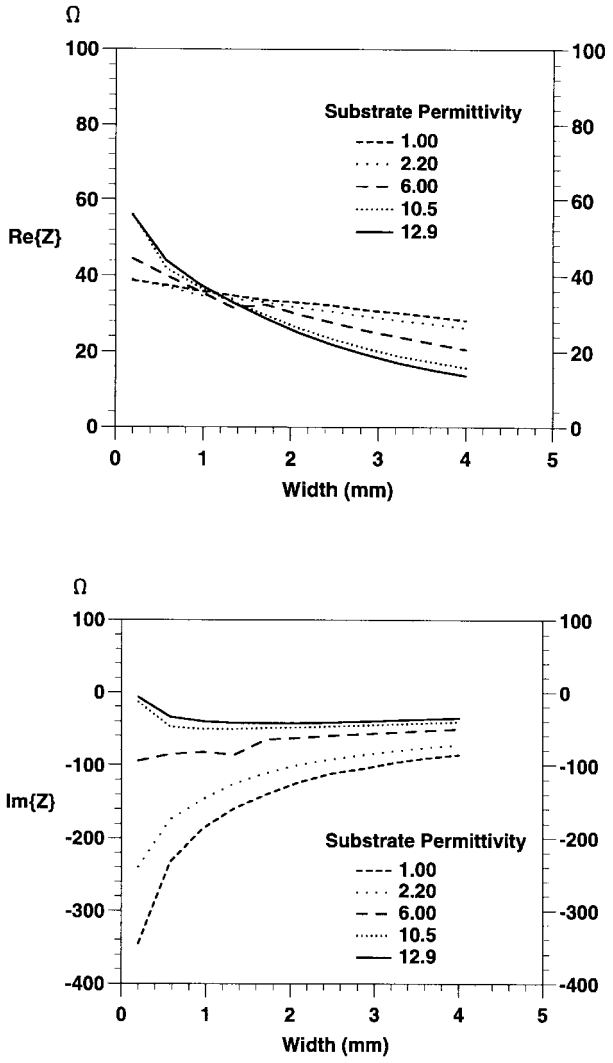

Fig. 9. The real and complex part of input impedance of a strip dipole antenna for different strip widths and substrate permittivities.

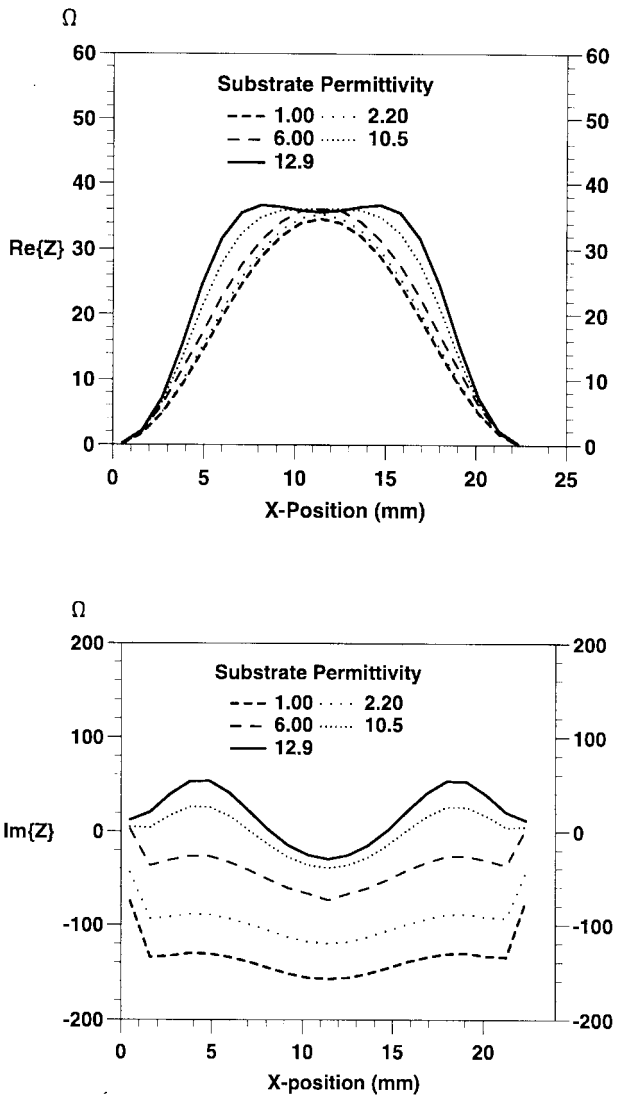

Fig. 10. The real and complex part of input impedance of a strip dipole antenna for different transverse strip positions and substrate permittivities.

the measurement due to field disturbance in the vicinity of the antenna.

Shorting the antenna-feed region and measuring from the two waveguide ports, the scattering from the so-formed planar strip is an alternative method for validating most of the modeling predictions. The difference between a MoM simulation for an impedance calculation and that for the scattering from the equivalent strips differs only in the excitation vector. Therefore, agreement between the measured and predicted scattering from the equivalent strip is taken as evidence that the associated antenna model is accurate.

The experimental data were obtained on an 8510C network analyzer with a short offset-short sliding-load calibration in WR-90 waveguide using the split-block test fixture shown in Fig. 12 to support the substrate in the waveguide. Additional de-embedding to move the measurement reference planes to the dielectric surface was performed using the ideal lossless propagation constant for WR-90 waveguide. All measurements are from 8.0 to 12.5 GHz with 401 data points. The three test structures were chosen to show the efficacy of the analysis for different permittivities and substrate thicknesses. A simulation

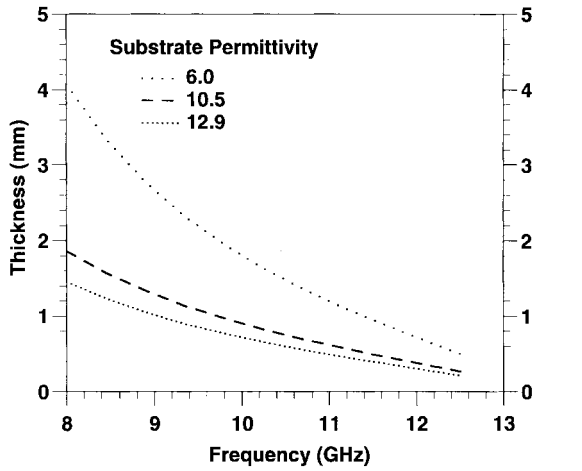

Fig. 11. The substrate thickness required to produce a transverse resonant as a function of frequency for different permittivities.

on thick, high dielectric constant material is included to show the presence of a substrate resonance.

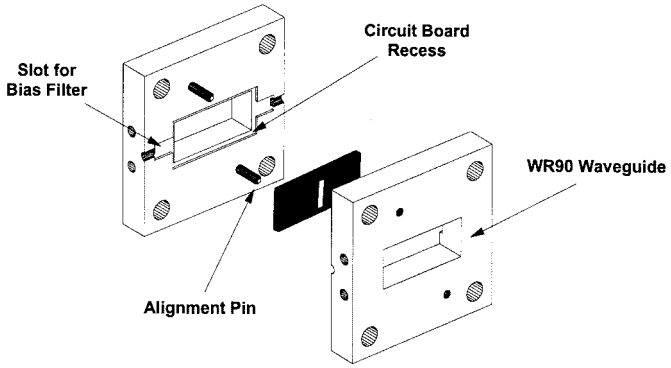

Fig. 12. The rectangular-waveguide test fixture.

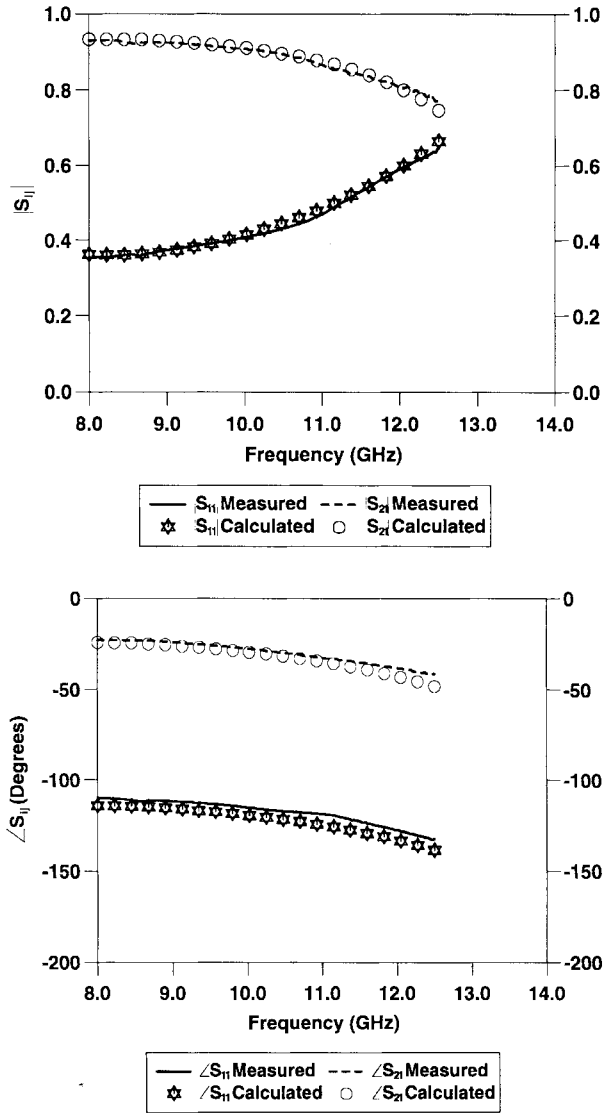

Fig. 13. The measured and MoM calculated scattering parameters from a shorted antenna 1-mm wide and 8-mm long, centered on 0.010-in-thick $\epsilon_{r=2.2}$ dielectric in WR-90 waveguide.

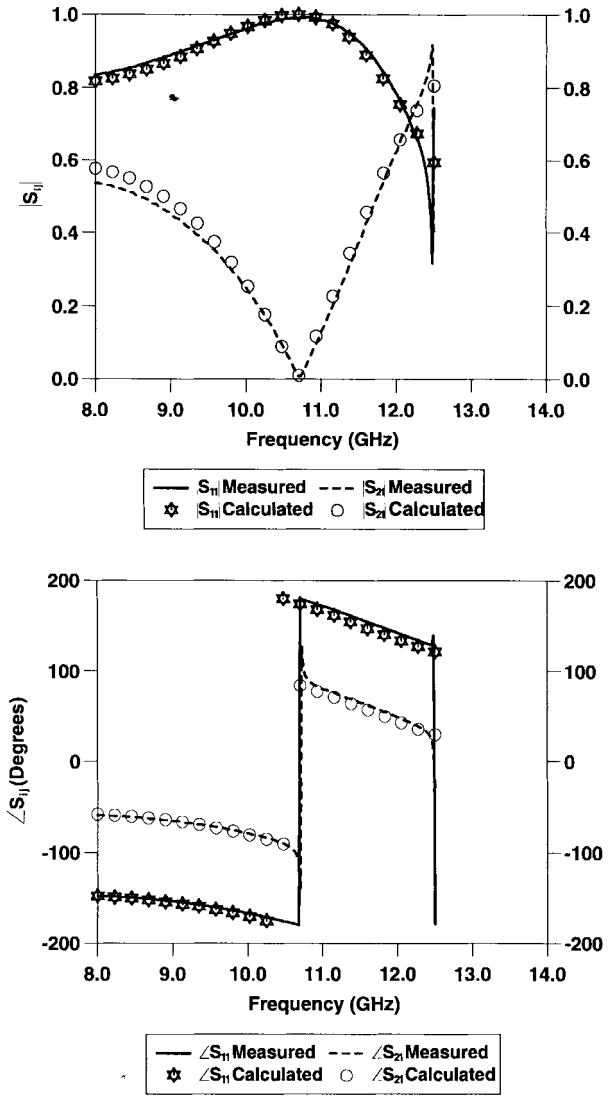

Fig. 14. The measured and MoM calculated scattering parameters from a shorted antenna 1-mm wide and 8-mm long centered on 0.010-in-thick $\epsilon_{r=6.0}$ dielectric in WR-90 waveguide.

These simulated data presented here for comparison with the experiment use $P = 3$ and $Q = 16$, and the calculation at each frequency point takes approximately 120 central processing unit (CPU) s on an HP-735 workstation. Fig. 13 shows the measured and predicted scattering from a shorted antenna 8-mm long and 1-mm wide centered on 0.010 in RT-Duroid 5880 ($\epsilon_r = 2.2$). Fig. 14 shows the measured and predicted scattering from the same shorted antenna structure centered on 0.010 in RT-Duroid 6010 ($\epsilon_r = 10.5$), while Fig. 15 shows the scattering behavior of the same shorted antenna on 0.025 in RT-Duroid 6006 ($\epsilon_r = 6.0$).

The measured and predicted data from the three test structures are generally in excellent agreement. On thin substrates below the resonant slab-mode frequency, there is little discrepancy between the data. However, on the thicker $\epsilon_r = 6.0$ material there is a slab-mode resonance at 11.90 GHz, close to the 12.05 GHz value as predicted by the theory of Section V. In the vicinity of this resonance there is strong coupling to the TE_0 slab mode and here the measurements and MoM predicted values diverge.

The excitation of a slab mode constrains the range of substrate thickness and permittivity that can be used in a given design. Other antenna shapes will couple to the slab modes in

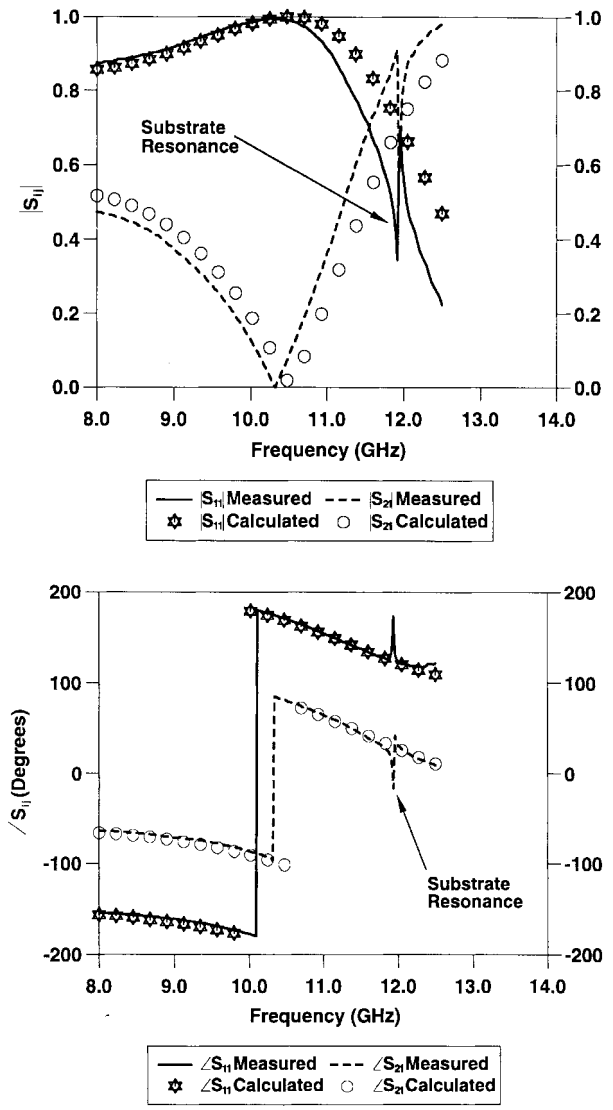

Fig. 15. The measured and MoM calculated scattering parameters from a shorted antenna 1-mm wide and 8-mm centered on 0.025-in-thick $\epsilon_{r=6.0}$ dielectric in WR-90 waveguide.

a different fashion, possibly exciting the TM_0 mode, while the present strip design appears to excite only the TE_0 mode. Although beyond the scope of this study, further investigation of this coupling is possible within the present integral-equation formulation through an additional integral equation for the dielectric slab coupled to the integral equations solved in this paper.

VII. Conclusion

A MoM analysis using Galerkin's method has been developed for strip dipole-antenna arrays located in rectangular waveguide. The analysis gives the frequency-dependent network matrix for the array with arbitrary terminations and has been used in the design of multiple-device oscillator power-combining circuits [8]. The analysis makes no assumptions about array symmetry or the nature of the current density on the surface of each antenna. With the aid of suitable meshing software, the effect of bias line and the analysis of antennas of more complex geometries can be undertaken with the same general full two-dimensional (2-D) analysis presented here.

Computational issues associated with the method were developed, and it was shown that the number of modes required in the summation of the doubly infinite series depends on the subsection size and must be closely monitored to achieve stable numerical results.

The general impedance behavior of single-strip dipole antennas was presented as a function of both geometrical and material parameters and gives some insight into array design for a given application as well as providing embedding impedance data suitable for planar mixers or oscillators. The existence of slab modes has been identified and a procedure for predicting a slab-mode resonance has been given. The numerical predictions show excellent agreement with experiment away from the slab-mode resonant frequencies validated using scattering measurements in the range of 8.0–12.5 GHz.

Appendix A
The Dyadic Green's Function for Infinite Rectangular Waveguide

Tai [20] has derived the dyadic Green's function for infinite rectangular waveguide. By adopting his notation with minor modification, the result is

$$\overline{\mathbf{G}}(\mathbf{r}|\mathbf{r}') = \frac{2\omega\mu_0}{ab}\sum_m\sum_n \frac{\bar{\epsilon}_{mn}}{k_c^2 k_g} \times \begin{cases} \mathbf{M_e}(k_g)\mathbf{M'_e}(-k_g) + \mathbf{N_o}(\mathbf{k_g})\mathbf{N'_o}(-\mathbf{k_g}) & z > z' \\ \mathbf{M_e}(-\mathbf{k_g})\mathbf{M'_e}(\mathbf{k_g}) + \mathbf{N_o}(-\mathbf{k_g})\mathbf{N'_o}(\mathbf{k_g}) & z < z' \end{cases} \tag{25}$$

where $k_c^2 = k_x^2 + k_y^2$, $k_x = m\pi/a$, and $k_y = n\pi/b$, $k_g = \sqrt{k_0^2 - k_c^2}$, ω is the angular frequency, $a \times b$ is the waveguide cross section, and $k_0 = \omega/c$ where c is the speed of light. Also, $\bar{\epsilon}_{mn} = \frac{1}{2}$ when one of $m, n = 0$, and zero otherwise, and the propagation constant $\gamma_{mn} = jk_g$. Furthermore,

$$\mathbf{M_e}(\pm k_g) = (-k_y \cos k_x x \sin k_y y\hat{x} + k_x \sin k_x x \cos k_y y\hat{y})e^{\pm\gamma_{mn}z} \tag{26}$$

$$\mathbf{N_o}(\pm k_g) = \frac{1}{k_0}(\pm\gamma_{mn}k_x \cos k_x x \sin k_y y\hat{x} \pm \gamma_{mn}k_y \sin k_x x \cos k_y y\hat{y} + k_c^2 \sin k_x x \sin k_y y\hat{z})e^{\pm\gamma_{mn}z}. \tag{27}$$

The functions $\mathbf{M_e}(k_g)$ and $\mathbf{N_o}(k_g)$ relate to the TE and TM rectangular-waveguide modes, respectively. Since by definition we are excluding $\hat{z}$-components of current, the G_{iz} where $i \in \{x, y, z\}$ terms of the dyadic are of no interest. Explicitly writing out the four relevant elements of the dyadic:

$$\mathbf{G_{xx}} = \frac{2jZ_0k_0}{ab}\sum_{m=0}^{\infty}\sum_{n=1}^{\infty}\frac{\bar{\epsilon}_{mn}}{k_c^2\gamma_{mn}} \times \left(k_y^2 - \frac{\gamma_{mn}^2 k_x^2}{k_0^2}\right)\cos k_x x \sin k_y y \times \cos k_x x' \sin k_y y' e^{\gamma_{mn}|z-z'|} \tag{28}$$

$$\mathbf{G_{xy}} = \frac{2jZ_0k_0}{ab}\sum_{m=1}^{\infty}\sum_{n=1}^{\infty}\frac{\bar{\epsilon}_{mn}}{k_c^2\gamma_{mn}} \times\left(-k_xk_y-\frac{\gamma_{mn}^2k_xk_y}{k_0^2}\right)\cos k_xx\sin k_yy \times\sin k_xx'\cos k_yy'e^{\gamma_{mn}|z-z'|} \tag{29}$$

$$\mathbf{G_{yx}} = \frac{2jZ_0k_0}{ab}\sum_{m=1}^{\infty}\sum_{n=1}^{\infty}\frac{\bar{\epsilon}_{mn}}{k_c^2\gamma_{mn}} \times\left(-k_xk_y-\frac{\gamma_{mn}^2k_xk_y}{k_0^2}\right)\sin k_xx\cos k_yy \times\cos k_xx'\sin k_yy'e^{\gamma_{mn}|z-z'|} \tag{30}$$

$$\mathbf{G_{yy}} = \frac{2jZ_0k_0}{ab}\sum_{m=1}^{\infty}\sum_{n=0}^{\infty}\frac{\bar{\epsilon}_{mn}}{k_c^2\gamma_{mn}} \times\left(k_x^2-\frac{\gamma_{mn}^2k_y^2}{k_0^2}\right)\sin k_xx\cos k_yy\sin k_xx' \times\cos k_yy'e^{\gamma_{mn}|z-z'|}. \tag{31}$$

APPENDIX B
THE ELEMENTS OF THE REACTION MATRIX

The reaction matrix takes the form

$$\begin{bmatrix} \begin{pmatrix} Z^1_{1_{xx}} & Z^1_{1_{xy}} \\ Z^1_{1_{yx}} & Z^1_{1_{yy}} \end{pmatrix} & \cdots & \begin{pmatrix} Z^1_{W_{xx}} & Z^1_{W_{xy}} \\ Z^1_{W_{yx}} & Z^1_{W_{yy}} \end{pmatrix} \\ \vdots & \ddots & \vdots \\ \begin{pmatrix} Z^W_{1_{xx}} & Z^W_{1_{xy}} \\ Z^W_{1_{yx}} & Z^W_{1_{yy}} \end{pmatrix} & \cdots & \begin{pmatrix} Z^W_{W_{xx}} & Z^W_{W_{xy}} \\ Z^W_{W_{yx}} & Z^W_{W_{yy}} \end{pmatrix} \end{bmatrix} \times\begin{bmatrix} J_{1_x} \\ J_{1_y} \\ \vdots \\ J_{W_x} \\ J_{W_y} \end{bmatrix} = \begin{bmatrix} \langle E_1, J_1\rangle \\ \langle E_2, J_2\rangle \\ \vdots \\ \langle E_{W-1}, J_{W-1}\rangle \\ \langle E_W, J_W\rangle \end{bmatrix} \tag{32}$$

which is a square matrix containing $W\times W$ submatrices—each a 2×2 matrix. Each of these 2×2 matrices contain the following number of elements:

$$\begin{bmatrix} \{Q(P-1)\times Q(P-1)\} & \{Q(P-1)\times P(Q-1)\} \\ \{P(Q-1)\times Q(P-1)\} & \{P(Q-1)\times P(Q-1)\} \end{bmatrix} \tag{33}$$

for Q–$\hat{y}$ sections and P–$\hat{x}$ sections on each antenna. Again, $Z^j_{i_{xy}}$ are the elements due to the x-component of the $\hat{y}$-directed electric field from the current on antenna i having been tested with the current elements on antenna j.

The elements of the reaction matrix are

$$Z^a_{b_{xx}} = F(\Delta x,\Delta x')\sum_{m=0}^{\infty}\sum_{n=1}^{\infty} \times\frac{\bar{\epsilon}_{mn}(k_y^2k_0^2\xi_{\rm te}-k_x^2\gamma_{mn}^2\xi_{\rm tm})}{k_c^2k_m^2k_m^2k_y^2\gamma_{mn}} \times\chi_1(k_x,\Delta x)\chi_1(k_x,\Delta x') \times\chi_2(k_y,\Delta y)\chi_2(k_y,\Delta y') \times\phi^a_{mn}(I_{xx},\Delta x,I_{yx},\Delta y) \times\phi^b_{mn}(I'_{xx},\Delta x',I'_{yx},\Delta y')$$

$$Z^a_{b_{xy}} = F(\Delta x,\Delta y')\sum_{m=1}^{\infty}\sum_{n=1}^{\infty} \times\frac{-(k_0^2\xi_{\rm te}+\gamma_{mn}^2\xi_{\rm tm})}{k_c^2k_m^2k_n^2\gamma_{mn}} \times\chi_1(k_x,\Delta x)\chi_1(k_y,\Delta y') \times\chi_2(k_y,\Delta y)\chi_2(k_x,\Delta x') \times\phi^a_{mn}(I_{xx},\Delta x,I_{yx},\Delta y) \times\psi^b_{mn}(I'_{xy},\Delta x',I'_{yx},\Delta y')$$

$$Z^a_{b_{yx}} = F(\Delta y,\Delta x')\sum_{m=1}^{\infty}\sum_{n=1}^{\infty} \times\frac{-(k_0^2\xi_{\rm te}+\gamma_{mn}^2\xi_{\rm tm})}{k_c^2k_m^2k_n^2\gamma_{mn}} \times\chi_1(k_y,\Delta y)\chi_1(k_x,\Delta x') \times\chi_2(k_x,\Delta x)\chi_2(k_y,\Delta y') \times\psi^a_{mn}(I_{xy},\Delta x,I_{yy},\Delta y) \times\phi^b_{mn}(I'_{xx},\Delta x',I'_{yx},\Delta y')$$

$$Z^a_{b_{yy}} = F(\Delta y,\Delta y')\sum_{m=1}^{\infty}\sum_{n=0}^{\infty} \times\frac{\bar{\epsilon}_{mn}(k_x^2k_0^2\xi_{\rm te}-k_y^2\gamma_{mn}^2\xi_{\rm tm})}{k_c^2k_n^2k_n^2k_x^2\gamma_{mn}} \times\chi_1(k_y,\Delta y)\chi_1(k_y,\Delta y') \times\chi_2(k_x,\Delta x)\chi_2(k_x,\Delta x') \times\psi^a_{mn}(I_{xy},\Delta x,I_{yy},\Delta y) \times\psi^b_{mn}(I'_{xy},\Delta x',I'_{yy},\Delta y')$$

where

$$F(\Delta i,\Delta j) = \frac{128jk_0Z_0}{ab\sin(k_0\Delta i)\sin(k_0\Delta j)}$$

$$\chi_1(k_i,\Delta i) = \sin\left[\frac{(k_i+k_0)\Delta i}{2}\right] \times\sin\left[\frac{(k_i-k_0)\Delta i}{2}\right]$$

$$\chi_2(k_i,\Delta i) = \sin\left(\frac{k_i\Delta i}{2}\right)$$

$$\phi^s_{mn}(I_{ii},\Delta i,I_{ij},\Delta j) = \cos[k_i(x_0^s+I_{ii}\Delta i)] \times\sin\{k_j[y_0^s+(I_{ij}-\tfrac{1}{2})\Delta j]\}$$

$$\psi^s_{mn}(I_{ij},\Delta i,I_{jj},\Delta j) = \cos[k_j(y_0^s+I_{jj}\Delta j)] \times\sin\{k_i[x_0^s+(I_{ij}-\tfrac{1}{2})\Delta i]\}.$$

If (α^s, β^s) is the center of the antenna s, then $(x_0^s, y_0^s) = (\alpha^s - w, \beta^s - l)$ where $2w$ is the antenna width and $2l$ is its length. Also $k_m^2 = k_x^2 - k_0^2$ and $k_n^2 = k_y^2 - k_0^2$. If the strip is subdivided into $P-\hat{x}$ and $Q-\hat{y}$ sections then integer variables I_{xx}, I'_{xx} are in the range 1: $(P-1)$, I_{xy}, I'_{xy} from 1: P, I_{yx}, I'_{yx} from 1: Q and I_{yy}, I'_{yy} from 1: $(Q-1)$.

ACKNOWLEDGMENT

The authors wish to thank T. Mosely and J. Shipman who provided the precision machining of the test fixtures. The authors also wish to thank the reviewers for their useful comments.

REFERENCES

[1] J. Mink, "Quasi-optical power combining of solid-state millimeter-wave sources," *IEEE Trans. Microwave Theory Tech.*, vol. MTT-34, pp. 273–279, Feb. 1986.
[2] Z. Popović *et al.*, "A 100-MESFET planar grid oscillator," *IEEE Trans. Microwave Theory Tech.*, vol. 39, pp. 193–199, Feb. 1991.
[3] R. Weikle, II *et al.*, "Planar MESFET grid oscillators using gate feedback," *IEEE Trans. Microwave Theory*, vol. 40, pp. 1997–2003, Nov. 1992.
[4] K. Moonil *et al.*, "A 100-element HBT grid amplifier," *IEEE Trans. Microwave Theory Tech.*, vol. 41, pp. 1762–1771, Oct. 1993.
[5] C.-M. Liu *et al.*, "Monolithic 40-GHz 670 mW HBT grid amplifier," in *Proc. IEEE Int. Microwave Symp.*, vol. 2, San Francisco, CA, June 1996, pp. 1123–1126.
[6] M. P. De Lisio *et al.*, "A 44–60 GHz monolithic pHEMT grid amplifier," in *Proc. IEEE Int. Microwave Symp.*, vol. 2, San Francisco, CA, June 1996, pp. 1127–1130.
[7] J. A. Higgins *et al.*, "44-GHz monolithic plane wave amplifiers," *IEEE Microwave Guided Wave Lett.*, vol. 5, pp. 347–348, Oct. 1995.
[8] A. R. Adams *et al.*, "Method of moments and time domain analyses of waveguide based hybrid multiple device oscillators," in *Proc. IEEE Int. Microwave Symp.*, vol. 3, San Francisco, CA, June 1996, pp. 1255–1258.
[9] R. Eisenhart and P. Khan, "Theoretical and experimental analysis of a waveguide mounting structure," *IEEE Trans. Microwave Theory Tech.*, vol. MTT-8, pp. 706–719, Aug. 1971.
[10] T. Itoh and R. Mittra, "Spectral-domain approach for calculating the dispersion characteristics of microstrip lines," *IEEE Trans. Microwave Theory Tech.*, vol. MTT-21, pp. 496–499, July 1973.
[11] J. C. Rautio and R. F. Harrington, "An electromagnetic time-harmonic analysis of shielded microstrip circuits," *IEEE Trans. Microwave Theory Tech.*, vol. MTT-35, pp. 726–730, Aug. 1987.
[12] A. Hill and V. K. Tripathi, "An efficient algorithm for the three-dimensional analysis of passive microstrip components and discontinuities for microwave and millimeter-wave integrated circuits," *IEEE Trans. Microwave Theory Tech.*, vol. 39, pp. 83–91, Jan. 1991.
[13] L.-W. Li *et al.*, "Input impedance of a probe-excited semi-infinite rectangular waveguide with arbitrary multilayered loads: Part I—Dyadic Green's functions," *IEEE Trans. Microwave Theory Tech.*, vol. 43, pp. 1559–1566, July 1995.
[14] S. Hashemi-Yeganeh and C. R. Birthcher, "Numerical and experimental studies of current distributions on thin metallic posts inside rectangular waveguides," *IEEE Trans. Microwave Theory Tech.*, vol. 42, pp. 1063–1068, June 1994.
[15] R. F. Harrington, *Field Computation by Moment Methods.* New York: Macmillan, 1968.
[16] V. H. Rumsey, "The reaction concept in electromagnetic theory," *Phys. Rev., Ser. 2,* vol. 94, pp. 1483–1491, 1954.
[17] L. P. Dunleavy and P. B. Katehi, "A generalized method for analyzing shielded thin microstrip discontinuities," *IEEE Trans. Microwave Theory Tech.*, vol. 36, pp. 1758–1766, Dec. 1988.
[18] G. V. Eleftheriades *et al.*, "Millimeter-wave integrated horn antennas: Part I: Theory," *IEEE Trans. Antennas Propagat.*, vol. 39, pp. 1575–1581, Nov. 1991.
[19] R. F. Harrington, *Time-Harmonic Electromagnetic Fields.* New York: McGraw-Hill, 1961.
[20] C.-T. Tai, *Dyadic Green's Functions in Electromagnetic Theory.* New York: Intext, 1971.

Andrew R. Adams was born in Sydney, Australia, in 1968. He received the B.Sc. and B.E. (Hons. I) degrees from the University of Sydney, Sydney, Australia, in 1989 and 1991, respectively, and Ph.D. degree from the University of Leeds, Leeds, U.K., in 1997.

In 1991, he worked as a Microwave Engineer with OTC Australia Research and Development, designing MMIC's and developing low-cost satellite-transmission systems. In 1992, he joined the CSIRO Division of Radiophysics as an RF Engineer, working on wireless systems at 40 GHz. In 1993, he joined the Microwave and Terahertz Technology Group, University of Leeds, working in the area of novel radiative power combiners. In 1997, he joined Standard Communications, Gladesville, N.S.W., Australia, as an RF Design Engineer. His interests include integral-equation formulations of electromagnetic problems, millimeter-wave power combining, and nonlinear dynamics.

Dr. Adams received a IEEE Microwave Theory and Techniques Society Graduate Fellowship in 1995 and 1996.

Roger D. Pollard (M'77–SM'91–F'97) was born in London, U.K., in 1946. He received the B.Sc. and Ph.D. degrees in electrical and electronic engineering from the University of Leeds, Leeds, U.K.

He currently holds the Hewlett-Packard Chair in high-frequency measurements in the School of Electronic and Electrical Engineering, University of Leeds, where he has been a Faculty Member since 1974. He is jointly responsible for the activities of the Institute of Microwave and Photonics, University of Leeds, which has over 40 active researchers, a strong graduate program, and has made contributions to microwave passive- and active-device research. His personal interests are in microwave-network measurements, calibration and error correction, microwave and millimeter-wave circuits, and large-signal and nonlinear characterization. He has been a consultant to the Hewlett-Packard Company, Santa Rosa, CA, since 1981.

Dr. Pollard is a Chartered Engineer and a member of the Institution of Electrical Engineers (IEE) (U.K.). He is serving his second term as an elected member of the IEEE Microwave Theory and Techniques Society Administrative Committee, where he is the 1997 vice president.

Christopher M. Snowden (S'82–M'82–SM'91–F'96) received the B.Sc., M.Sc., and Ph.D. degrees from the University of Leeds, Leeds, U.K., in 1977, 1979, and 1982, respectively.

In 1977, he worked as an Applications Engineer for Mullard, Mitcham. In 1982, he was appointed Lecturer in the Department of Electronics, University of York, York, U.K. He joined the Microwave and Solid State Group, Department of Electrical and Electrical Engineering, University of Leeds, in 1983. He currently holds the Chair of Microwave Engineering in the Institute of Microwaves and Photonics, University of Leeds, and is also Head of the School of Electronic and Electrical Engineering. In 1987, he was a Visiting Research Associate at the California Institute of Technology at Pasadena. He has been a Consultant to M/A-Com Inc., Corporate Research and Development since 1989, while on sabbatical leave from 1990 to 1991. During that time, he represented M/A-Com as Senior Staff Scientist. He is a Member of the MIT Electromagnetics Academy, a top scientist at the International Research Center for Telecommunications-Transmission and Radar, Delft University of Technology, The Netherlands, and founding member of the International GaAs Simulation Group. He has written seven books and over 175 papers. His main research interests include compound semiconductor device modeling, microwave, terahertz, and optical nonlinear subsystem design, and advanced semiconductor devices.

Dr. Snowden is a distinguished lecturer (1996/1997) for the IEEE Electron Devices Society, and was chairman of the 1995 International Microwaves and RF Conference.